LA-UR- 00-4497

Approved for public release; distribution is unlimited.

Title: Comparison of Recursive Estimation Techniques for Position Tracking of Radioactive Sources

Author(s): Ken Muske and James Howse

Submitted to: American Control Conference 2001

Los Alamos
NATIONAL LABORATORY

ACC01-AICHE602

Comparison of Recursive Estimation Techniques for Position Tracking Radioactive Sources

Kenneth R. Muske
Department of Chemical Engineering, Villanova University, Villanova, PA 19085-1681

James W. Howse
Computational Science Methods, Los Alamos National Laboratory, Los Alamos, NM 87545

Abstract

This paper compares the performance of recursive state estimation techniques for tracking the physical location of a radioactive source within a room based on radiation measurements obtained from a series of detectors at fixed locations. Specifically, the extended Kalman filter, algebraic observer, and nonlinear least squares techniques are investigated. The results of this study indicate that recursive least squares estimation significantly outperforms the other techniques due to the severe model nonlinearity.

1. Introduction

The position tracking system consists of a single radioactive source of known strength and initial position within a room containing four radiation detectors. The radiation detectors are located at fixed positions on each wall of the room and provide discrete count rate measurements at a one second sample period. The count rate for a given sensor represents the total number of gamma-energy photons detected by that sensor over the one second sample period. We wish to track the position of the source in real time as it is moved within the room based on the radiation detector measurements. The estimate of the source location is based on a nonlinear model for each sensor that relates the detector count rate to location.

2. Dynamic Model

The state of the system, $\boldsymbol{s} = [x\ y\ z\ \mathcal{B}]^T$, consists of the x–y–z coordinates of the position of the source within the room and the background radiation, $\mathcal{B}$, which also changes. Since the background radiation does not vary significantly and the source is normally stationary in practice with no prescibed trajectory when it is moved, we choose to model the state dynamics as a random walk process in which $\boldsymbol{\omega}$ is an independant, normally distributed disturbance vector.

$$\dot{\boldsymbol{s}} = 0 + \boldsymbol{\omega} \tag{1}$$

The system measurements consist of the count rates, $\boldsymbol{\mathcal{M}} = [\mathcal{M}_1\ \mathcal{M}_2\ \mathcal{M}_3\ \mathcal{M}_4]^T$, from the four radiation detectors in which the subscript indicates the detector. The count rate measured by the ith detector can be determined from the source strength, detector properties, and the state of the system from the following relationship [1]

$$\mathcal{M}_i = \frac{\Omega_i\, \mathcal{S}\, \epsilon_i\, \mathcal{F}_i + \mathcal{B}}{1 + \tau_i\, \Omega_i\, \mathcal{S}\, \epsilon_i\, \mathcal{F}_i} + \nu_i, \quad i = 1, \ldots, 4 \tag{2}$$

in which $\mathcal{S}$ is the source strength in counts per second, $\epsilon_i = 0.1$ is the detector efficiency, $\tau_i = 3.3$ nsec is the detector dead time, $\mathcal{F}_i$ is the product of all correction factors such as absorption and backscattering which is assumed to be unity for each detector in this work, $\mathcal{B}$ is the number of counts per second which constitutes the background radiation, and $\boldsymbol{\nu}$ is an independent, Poisson distributed measurement noise vector.

The view factor for each detector, Ω_i, is the ratio of the number of particles which actually enter the detector to the total number of particles emitted by the source. Assuming a point source located at coordinates (u, v, w) relative to the detector and a detector of width $\mathcal{W}$ and height $\mathcal{H}$, the quantity Ω_i can be determined as the solid angle subtended by the detector [2]

$$\begin{aligned} \Omega_i(u_i, v_i, w_i) &= \tan^{-1}\left(\frac{u_i\, v_i}{|w_i|\, \sqrt{u_i^2 + v_i^2 + w_i^2}}\right) \\ &- \tan^{-1}\left(\frac{(u_i - \mathcal{W})\, v_i}{|w_i|\, \sqrt{(u_i - \mathcal{W})^2 + v_i^2 + w_i^2}}\right) \\ &- \tan^{-1}\left(\frac{u_i\, (v_i - \mathcal{H})}{|w_i|\, \sqrt{u_i^2 + (v_i - \mathcal{H})^2 + w_i^2}}\right) \\ &+ \tan^{-1}\left(\frac{(u_i - \mathcal{W})\, (v_i - \mathcal{H})}{|w_i|\, \sqrt{(u_i - \mathcal{W})^2 + (v_i - \mathcal{H})^2 + w_i^2}}\right) \end{aligned} \tag{3}$$

in which $\mathcal{H} = 0.253$ m and $\mathcal{W} = 0.914$ m for the detectors used in this study. The expression in

Eq. 3 is based on a detector-centered coordinate system. Since there are four detectors in this study, it is not possible to choose a coordinate system that is centered at each detector. Therefore, we choose a room-centered coordinate system to describe the source location and determine a coordinate transformation from room-centered to detector-centered coordinates for each detector. The required transformation, which converts room-centered coordinates, (x, y, z), to detector-centered coordinates, (u_i, v_i, w_i), for the ith detector, is linear and can be expressed in matrix form as

$$\begin{pmatrix} u_i \\ v_i \\ w_i \end{pmatrix} = \begin{pmatrix} \cos\mathcal{A}_i & 0 & \sin\mathcal{A}_i & \begin{matrix}\mathcal{T}_{x,i}\cos\mathcal{A}_i + \\ \mathcal{T}_{z,i}\sin\mathcal{A}_i\end{matrix} \\ 0 & 1 & 0 & \mathcal{T}_{y,i} \\ -\sin\mathcal{A}_i & 0 & \cos\mathcal{A}_i & \begin{matrix}\mathcal{T}_{z,i}\cos\mathcal{A}_i - \\ \mathcal{T}_{x,i}\sin\mathcal{A}_i\end{matrix} \end{pmatrix} \begin{pmatrix} x \\ y \\ z \\ 1 \end{pmatrix} \tag{4}$$

in which $\mathcal{T}_{x,i}$, $\mathcal{T}_{y,i}$, and $\mathcal{T}_{z,i}$ are the translations along the room centered x, y, and z directions, respectively, and $\mathcal{A}_i$ is the rotation angle around the v-axis for the ith detector. Note that the source strength $\mathcal{S}$ and the background radiation $\mathcal{B}$ are invariant under this coordinate transformation.

3. Extended Kalman Filter

The extended Kalman filter computes a state estimate at each sampling period by the application of linear Kalman filtering on a linearized model of the nonlinear system about the current state estimate. This technique is justified if there exists a sufficiently large neighborhood in which the linearized model is a good representation of the nonlinear system. If, in addition, the disturbances are well represented by zero mean Gaussian state and measurement noise, the optimal estimate for the linearized system should be a reasonable approximation to the optimal estimate for the nonlinear system. Application of the extended Kalman filtering to a tracking problem is discussed in [3].

For the tracking system model presented in Section 2, only the sensor model in Eq. 2 is nonlinear. A linear approximation of this sensor model for use in the extended Kalman filter can be developed using the first order terms of a Taylor series expansion

$$\tilde{\boldsymbol{\mathcal{M}}}(\boldsymbol{s} + \boldsymbol{d}) = \boldsymbol{\mathcal{M}}(\boldsymbol{s}) + \boldsymbol{\mathcal{G}}\boldsymbol{d} \tag{5}$$

in which $\boldsymbol{\mathcal{M}}(\boldsymbol{s})$ is the sensor function evaluted at the state $\boldsymbol{s}$ and $\boldsymbol{\mathcal{G}}$ is the Jacobian matrix of the sensor model function evaluted at the state $\boldsymbol{s}$.

$$\boldsymbol{\mathcal{G}} = \begin{pmatrix} \frac{\partial \mathcal{M}_1}{\partial x} & \frac{\partial \mathcal{M}_1}{\partial y} & \frac{\partial \mathcal{M}_1}{\partial z} & \frac{\partial \mathcal{M}_1}{\partial \mathcal{B}} \\ \vdots & \vdots & \vdots & \vdots \\ \frac{\partial \mathcal{M}_4}{\partial x} & \frac{\partial \mathcal{M}_4}{\partial y} & \frac{\partial \mathcal{M}_4}{\partial z} & \frac{\partial \mathcal{M}_4}{\partial \mathcal{B}} \end{pmatrix} \tag{6}$$

$$\begin{aligned} \frac{\partial \mathcal{M}_i}{\partial x} &= \frac{\partial \mathcal{M}_i}{\partial \Omega_i}\left(\frac{\partial \Omega_i}{\partial u_i}\frac{\partial u_i}{\partial x} + \frac{\partial \Omega_i}{\partial v_i}\frac{\partial v_i}{\partial x} + \frac{\partial \Omega_i}{\partial w_i}\frac{\partial w_i}{\partial x}\right) \\ \frac{\partial \mathcal{M}_i}{\partial y} &= \frac{\partial \mathcal{M}_i}{\partial \Omega_i}\left(\frac{\partial \Omega_i}{\partial u_i}\frac{\partial u_i}{\partial y} + \frac{\partial \Omega_i}{\partial v_i}\frac{\partial v_i}{\partial y} + \frac{\partial \Omega_i}{\partial w_i}\frac{\partial w_i}{\partial y}\right) \\ \frac{\partial \mathcal{M}_i}{\partial z} &= \frac{\partial \mathcal{M}_i}{\partial \Omega_i}\left(\frac{\partial \Omega_i}{\partial u_i}\frac{\partial u_i}{\partial z} + \frac{\partial \Omega_i}{\partial v_i}\frac{\partial v_i}{\partial z} + \frac{\partial \Omega_i}{\partial w_i}\frac{\partial w_i}{\partial z}\right) \end{aligned}$$

3.1. First Order Filter

The first order filter uses the approximate sensor model in Eq. 5, linearized about the current state estimate, to construct a time-varying Kalman filter at each sampling period. The estimate of the state at sample time k give sensor measurements up to time k, $\hat{\boldsymbol{s}}_{k|k}$, is computed as follows

$$\begin{aligned} \hat{\boldsymbol{s}}_{k|k} &= \hat{\boldsymbol{s}}_{k|k-1} + \boldsymbol{d}_k & (7) \\ \boldsymbol{d}_k &= \boldsymbol{L}_k\left(\boldsymbol{\mathcal{D}}_k - \boldsymbol{\mathcal{M}}_{k|k-1}\right) & (8) \\ \hat{\boldsymbol{s}}_{0|0} &= [x_i\ y_i\ z_i\ \mathcal{B}_i]^T & (9) \end{aligned}$$

in which $\boldsymbol{\mathcal{D}}_k$ is the sensor measurement vector at sample time k, $\boldsymbol{\mathcal{M}}_{k|k-1}$ is the sensor model in Eqs. 2– 4 evaluted at the state estimate $\boldsymbol{s}_{k|k-1}$, and $\boldsymbol{s}_{0|0}$ is the known initial state. The time-varying linear Kalman filter gain at sample time k, $\boldsymbol{L}_k$, is determined by

$$\boldsymbol{L}_k = \boldsymbol{P}_{k|k-1}\boldsymbol{\mathcal{G}}^T_{k|k-1}\left(\boldsymbol{\mathcal{G}}_{k|k-1}\boldsymbol{P}_{k|k-1}\boldsymbol{\mathcal{G}}^T_{k|k-1} + \boldsymbol{R}\right) \tag{10}$$

in which $\boldsymbol{\mathcal{G}}_{k|k-1}$ is the Jacobian matrix in Eq. 6 evaluated at the state estimate $\boldsymbol{s}_{k|k-1}$ and $\boldsymbol{P}_{k|k-1}$ is the estimated state covariance matrix. The estimated covariance of the state is updated at each sample time due to the contribution of the discrete measurement as follows.

$$\boldsymbol{P}_{k|k} = \left(\boldsymbol{I} - \boldsymbol{L}_k\boldsymbol{\mathcal{G}}_{k|k-1}\right)\boldsymbol{P}_{k|k-1} \tag{11}$$

The estimated state and state covariance matrix are updated between sampling times based on the dynamic model presented in Eq. 1.

$$\begin{aligned} \hat{\boldsymbol{s}}_{k+1|k} &= \hat{\boldsymbol{s}}_{k|k} & (12) \\ \boldsymbol{P}_{k+1|k} &= \boldsymbol{P}_{k|k} + \boldsymbol{Q} & (13) \end{aligned}$$

The tuning parameters for the filter are the state and measurement noise covariance matrices. Since the radiation detector measurement noise is Poisson distributed, the measurement covariance used for the filter is a diagonal matrix in which each diagonal entry is determined from the model predicted count rate at the current estimate of the state scaled by the dispersion. The state disturbance covariance matrix is taken as the identity matrix.

$$\begin{aligned} \boldsymbol{R} &= \mathsf{diag}[\gamma^2\boldsymbol{\mathcal{M}}_{k|k-1}] & (14) \\ \boldsymbol{Q} &= \boldsymbol{I} & (15) \end{aligned}$$

Figures 1 and 2 present the x-direction and y-direction tracking errors for the first order extended Kalman filter applied to the test data set. A value of $\gamma = 10$ was used to obtain these results. Larger values of γ resulted in poorer tracking performance while larger values resulted in instability of the estimator. As shown in these figures, the filter is unable to adequately track the source and places it outside of the room for a significant period during the test. The application of position constraints to the estimate at each sampling period does prevent state estimates outside of the room, but does not improve the prediction error significantly.

The constraints on the state estimate are imposed to prevent the estimated position from being outside the room and the estimated background from exceeding the historical bounds for the background levels in the room. The constraints on the change in the estimate at each sample period are imposed in order to keep measurement noise from changing the position excessively from time step to time step. Conceptually these constraints are reasonable since the source is moved by a person and there is a limit to how far a person can move in a given time interval.

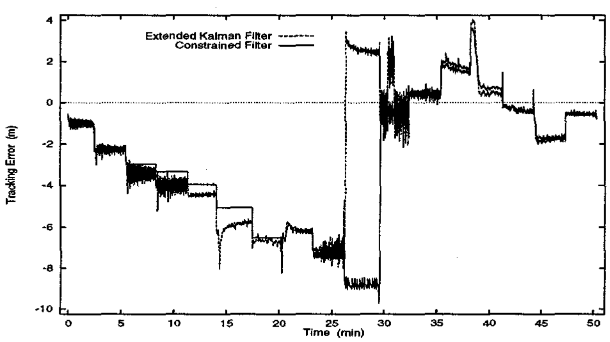

Figure 1: Extended filter x-direction tracking error.

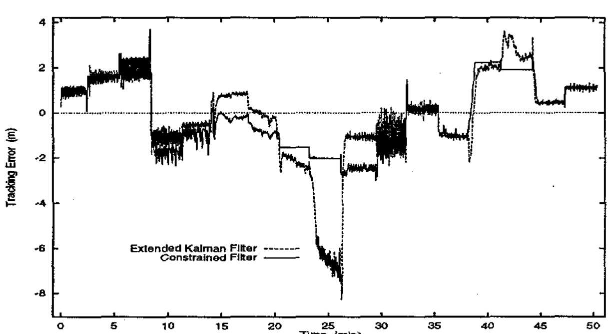

Figure 2: Extended filter y-direction tracking error.

3.2. Iterative Filter

Iterative extended Kalman filters have been developed in which a linearized model is determined from an updated state estimate at each iteration. These schemes attempt to reduce the estimation error by improving the approximation to the nonlinear system that is used in the determination of the filtered state. An iterative scheme that is used to compensate for nonlinearity in the measurement function is to repeat the calculation of $\hat{s}_{k|k}$ in Eq. 7 [4]. Letting $\hat{s}_{k|k}(i)$ represent the ith iterate of the filtered state estimate, the next iteration is determined as follows

$$
\begin{aligned}
\hat{s}_{k|k}(i+1) &= \hat{s}_{k|k-1} + \boldsymbol{d}_k(i) && (16)\\
\boldsymbol{d}_k(i) &= \boldsymbol{L}_k(i)\left(\boldsymbol{\mathcal{D}}_k - \boldsymbol{\mathcal{M}}_{k|k}(i) - \right. \\
&\qquad \left. \boldsymbol{\mathcal{G}}_{k|k}(i)\left(\hat{s}_{k|k-1} - \hat{s}_{k|k}(i)\right)\right) && (17)\\
\hat{s}_{k|k}(0) &= \hat{s}_{k|k-1} && (18)
\end{aligned}
$$

in which the filter gain, $\boldsymbol{L}_k(i)$, and the Jacobian of the sensor model function, $\boldsymbol{\mathcal{G}}_{k|k}(i)$, are recomputed at each iteration based on the current iterate of the filtered state. The iteration is repeated until there is no significant difference between the iterated filtered states. The estimated state covariance is then updated in the same manner as Eq. 11 using the converged filter gain and sensor model function Jacobian. The estimated state and covariance are propagated between sampling times in the same manner as the first order filter. Note that a single iteration of this filter results in the first order extended Kalman filter.

The results for the iterative extended Kalman filter are shown in Figures 3 and 4 for the x-direction and y-direction tracking errors. A value of $\gamma = 10$ was used to obtain these results with a maximum of ten iterations allowed to get within a 0.1 m tolerance for the 2-norm of the difference between sucessive iterates. An average of 7.5 iterations were required for the unconstrained filter and 6 iterations for the constrained filter. In both cases, however, most of the estimates either converged within two to three iterations or did not converge within the ten iteration limit. Figures 5 and 6 compare the performance of the constrained first order extended Kalman filter and the constrained iterative filter. As shown in these figures, the improvement in the iterated filter tracking error is modest for almost an order of magnitude increase in computational effort. Based on these results, successive linearization of the sensor model function does not result in a converged state estimate and does not significantly improve the state estimate tracking error over the first order filter.

4. Algebraic Estimator

In this approach, the state of the system at each sample time is estimated by solving the nonlinear system of equations for the unknown state at sample period k, s_k.

$$\boldsymbol{\mathcal{M}}_k(s_k) - \boldsymbol{\mathcal{D}}_k = 0 \qquad (19)$$

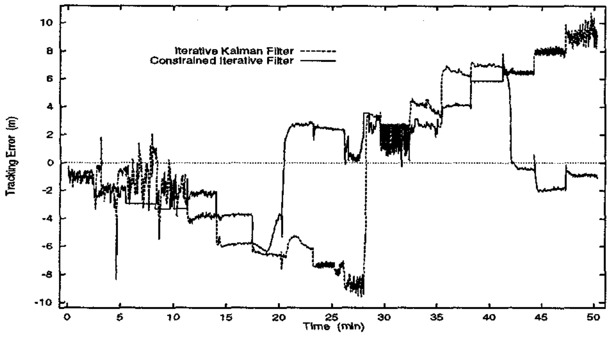

Figure 3: Iterative filter x-direction tracking error.

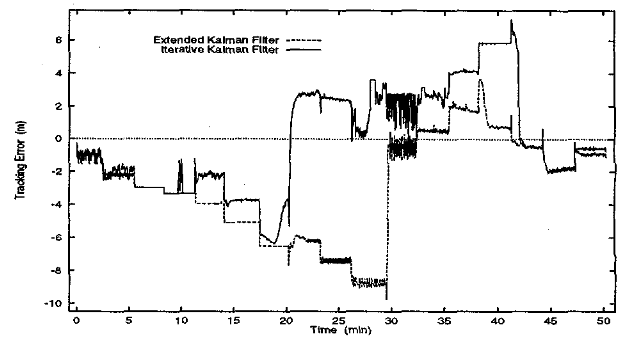

Figure 5: Constrained x-direction tracking error.

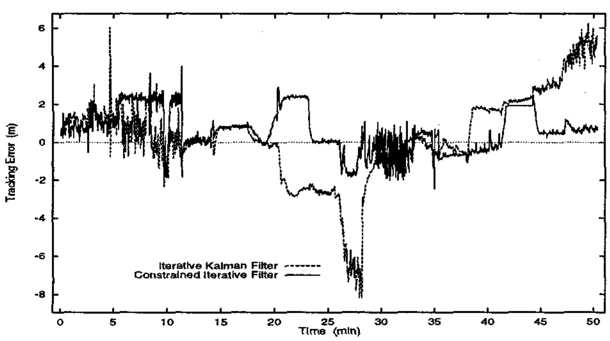

Figure 4: Iterative filter y-direction tracking error.

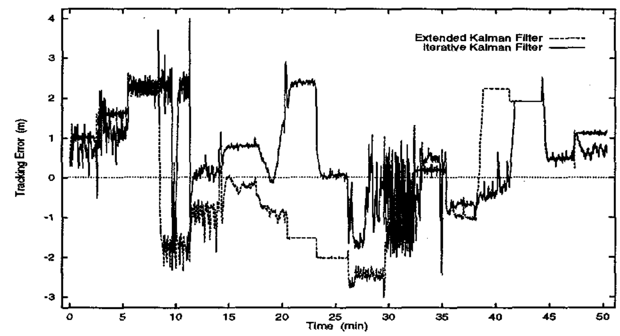

Figure 6: Constrained y-direction tracking error.

Moraal and Grizzle [5] employ Newton's method to solve the system of nonlinear equations generated by the algebraic state estimation problem. The Jacobian matrix required for Newton's method on this system of equations is that given in Eq. 6.

Newton's method applied to the system of nonlinear equations generated by the position tracking state estimation problem in Eq. 19 usually diverges when the previous state estimate is the starting point. This behavior suggests that the region of convergence is quite small and that the initial Newton direction is a poor search direction. This observation also helps explain the lack of significant improvement for the iterated extended Kalman filter. Since our attempt to use an unmodified Newton's method failed, we modified the approach suggested in [5] to start with five iterations of a gradient descent method and then switch to a Newton's method modified to converge globally for all succeeding iterations. This procedure did consistently produce a state estimate, but converged very slowly. Since this method does not explicitly consider disturbances, a number of the estimates produced by this procedure were outside of the room due to sensor measurement noise and modeling error. The incorporation of position constraints on the estimates at each sample period does prevent the algorithm from producing physically unrealistic estimates due to measurement noise, but the tracking performance was no better that the extended Kalman filter. The modifications necessary to consistently achieve a state estimate using this approach also required significantly more computational effort than the iterative filter.

5. Nonlinear Least Squares Estimator

A nonlinear least squares estimator that explicitly considers noise and constraints is considered in this section. At each sample time k, the optimal estimated change in the state, $\boldsymbol{d}_k$, is determined from the solution to the following optimization problem

$$\boldsymbol{d}_k^* = \arg\min_{\boldsymbol{d}_k} \left(\sum_{i=1}^{4} \mathcal{W}_i^m \Big(\mathcal{D}_i - \mathcal{M}_i \big(\hat{\boldsymbol{s}}_{k|k-1} + \boldsymbol{d}_k \big) \Big)^2 + \sum_{j=1}^{4} \mathcal{W}_j^d \, d_j^2(k) \right) \quad (20)$$

subject to

$$\begin{aligned} -\mathfrak{R}_j \le d_j(k) \le \mathfrak{R}_j, \\ \mathfrak{L}_j \le \hat{s}_j(k \mid k-1) + d_j(k) \le \mathfrak{U}_j, \end{aligned} \quad j = 1, \dots, 4$$

in which $\mathcal{W}_i^m$ is a weight that determines how closely the algorithm tries to match the model and $\mathcal{W}_j^d$ weights how much the algorithm changes the previous state estimate. We select $\mathcal{W}_i^m$ as the diagonal entries of the matrix $\boldsymbol{R}^{-1}$, defined in Eq. 14, and $\mathcal{W}_j^d$ as the diagonal entries of the matrix $\boldsymbol{Q}^{-1}$ in Eq. 15. The constraints are the same as those used in the

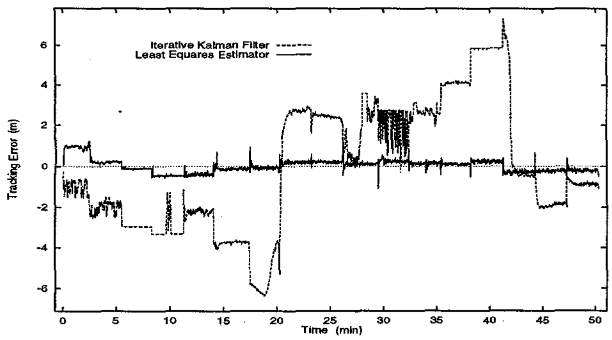

Figure 7: Constrained x-direction tracking error.

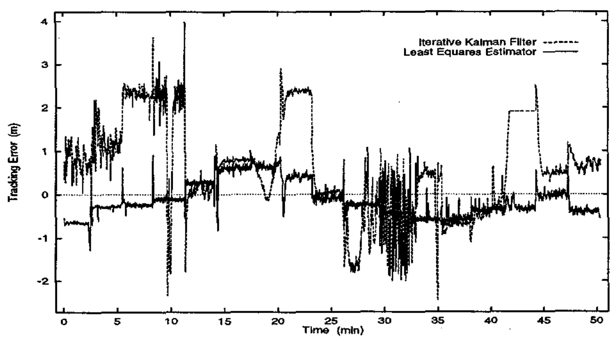

Figure 8: Constrained y-direction tracking error.

previous estimation techniques. For this estimator, the constraints are explicitly considered in the determination of the state estimate as opposed to being applied after the estimate is computed.

Figures 7 and 8 compare the x-direction and y-direction tracking error for the least squares estimator and the constrained, iterative filter. As shown in these figures, the least squares estimator performance is significantly better than the extended Kalman filtering approaches. The optimization in Eq. 20 was generally solved within the one second sampling period using CFSQP [6]. This algorithm uses a sequential quadratic programming approach modified so that each iteration is feasible with respect to the constraints. We chose this algorithm because all of the intermediate iterates of the algorithm are feasible. If it is necessary to stop the optimization before achieving convergence, the resulting suboptimal solution will still satisfy the constraints. Since the state dynamics are modeled as a random walk process, there is no advantage to a moving horizon estimator. Increasing the prediction horizon from one had essentially no effect on the tracking error.

Table 1 presents the 2-norm of the tracking error profile of each direction for each estimator presented in this work. The least squares estimator outperforms each of the other algorithms by a significant margin for x-direction and y-direction, which are the most important coordinates for source tracking. Figure 9 presents the change in the background radiation for each of the constrained estimators. In addition to a significant position tracking error, the linearized filters also estimate an unrealistic increase in the background radiation during the test.

Estimator	x (m)	y (m)	z (m)	$\mathcal{B}$ (count/sec)
First Order	208.8	110.9	45.5	6.14×10^4
First Order(c)	231.5	84.0	36.8	6.11×10^4
Iterative	314.2	128.4	47.6	7.37×10^4
Iterative(c)	172.6	69.3	76.9	4.74×10^4
Least Squares	17.8	23.8	19.5	1.53×10^3

Table 1: Tracking errors. (c) = constrained estimator.

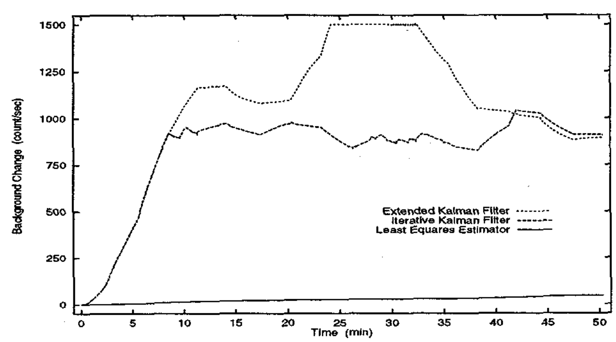

Figure 9: Estimated background radiation change.

References

[1] N. Tsoulfanidis. *Measurement and Detection of Radiation.* Nuclear Engineering Series. McGraw-Hill, Inc., New York, NY, 1983.

[2] H. Gotoh and H. Yagi. Solid angle subtended by a rectangular slit. *Nuclear Instruments and Methods*, 96(2):485–486, 1971.

[3] A. Gelb, editor. *Applied Optimal Estimation.* The M.I.T. Press, Cambridge, Massachusetts, 1974.

[4] A.H. Jazwinski. *Stochastic Processes and Filter Theory*, volume 64 of *Mathematics in Science and Engineering.* Academic Press, Inc., New York, NY, 1970.

[5] P. E. Moraal and J. W. Grizzle. Observer design for nonlinear systems with discrete-time measurements. *IEEE TAC*, 40(3):395–404, 1995.

[6] C.T. Lawrence, J.L. Zhou, and A.L. Tits. User's guide for CFSQP. Technical Report TR–94–16r1, Institute for Systems Research, University of Maryland, College Park, MD, 1994.